

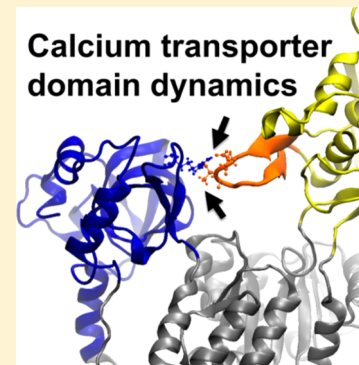
A Structural Mechanism for Calcium Transporter Headpiece Closure

Nikolai Smolin and Seth L. Robia*

Department of Cell and Molecular Physiology, Stritch School of Medicine, Loyola University Chicago, Maywood, Illinois 60153, United States

Supporting Information

ABSTRACT: To characterize the conformational dynamics of sarcoplasmic reticulum (SR) calcium pump (SERCA) we performed molecular dynamics simulations beginning with several different high-resolution structures. We quantified differences in structural disorder and dynamics for an open conformation of SERCA versus closed structures and observed that dynamic motions of SERCA cytoplasmic domains decreased with decreasing domain–domain separation distance. The results are useful for interpretation of recent intramolecular Förster resonance energy transfer (FRET) distance measurements obtained for SERCA fused to fluorescent protein tags. Those previous physical measurements revealed several discrete structural substates and suggested open conformations of SERCA are more dynamic than compact conformations. The present simulations support this hypothesis and provide additional details of SERCA molecular mechanisms. Specifically, all-atoms simulations revealed large-scale translational and rotational motions of the SERCA N-domain relative to the A- and P-domains during the transition from an open to a closed headpiece conformation over the course of a 400 ns trajectory. The open-to-closed structural transition was accompanied by a disorder-to-order transition mediated by an initial interaction of an N-domain loop ($\text{N}\beta 5-\beta 6$, residues 426–436) with residues 133–139 of the A-domain. Mutation of three negatively charged N-domain loop residues abolished the disorder-to-order transition and prevented the initial domain–domain interaction and subsequent closure of the cytoplasmic headpiece. Coarse-grained molecular dynamics simulations were in harmony with all-atoms simulations and physical measurements and revealed a close communication between fluorescent protein tags and the domain to which they were fused. The data indicate that previous intramolecular FRET distance measurements report SERCA structure changes with high fidelity and suggest a structural mechanism that facilitates the closure of the SERCA cytoplasmic headpiece.



INTRODUCTION

Oscillations in free cytosolic Ca^{2+} govern the relaxation and contraction of muscles. This Ca^{2+} cycle is the result of the coordinated actions of channels in the sarcoplasmic reticulum (SR) membrane, which release Ca^{2+} into the cytoplasm during contraction, and the SR calcium pump (SERCA),¹ which transports Ca^{2+} ions back into the SR to allow muscle relaxation. In the heart, disordered SERCA expression, function, and regulation are linked to cardiac disease, motivating investigation of SERCA structure/function mechanisms as a path to new therapeutic interventions. One important aspect of SERCA function is the large amplitude conformational changes that occur during the transport cycle.^{2–7} In particular, the role of domain dynamics in ion transport has been vividly illustrated by X-ray crystallography of SERCA. Several X-ray structures obtained for different catalytic substates are provided in Figure 1A, which shows the SERCA transmembrane domain (TM, gray) and the three cytosolic domains: nucleotide-binding (N, yellow), phosphorylation (P, black) and actuator (A, blue).⁸ These and other structure solutions reveal that translations and rotations of these cytosolic domains accompany the transport of ions from the cytosolic side to the luminal side of the sarcoplasmic reticulum membrane.^{9–11} Even though many such high-resolution structures are available, there are also likely to be

undiscovered states that will continue to resist crystallization because they are short-lived intermediate conformations or because they are structurally dynamic. For example, while there are many crystal structures showing a closed, compact headpiece, there is a paucity of structural information for SERCA in the open state. It has been suggested that this is because open structures only occur in the (nonphysiological) absence of nucleotide.¹² However, our previous FRET studies indicate significant population of open headpiece conformations *in vitro* and in live cardiac muscle cells.¹³ Thus, we consider it likely that there are other open structures, unsuitable for crystallization, which may be discovered with alternative approaches. Investigation of novel states and the structural mechanisms driving transitions between different states has benefitted from computational modeling.^{14–21} Molecular dynamics (MD) studies have revealed possible transition pathways for a large-scale open-to-closed conformational change^{15,22} and predicted novel intermediate states including an E1 2K⁺ conformation that has a very open headpiece architecture.²¹ Other studies used coarse-grained molecular dynamics (CGMD) to investigate E2 to E1 and E1P to E2P

Received: November 14, 2014

Revised: December 18, 2014

Published: December 22, 2014

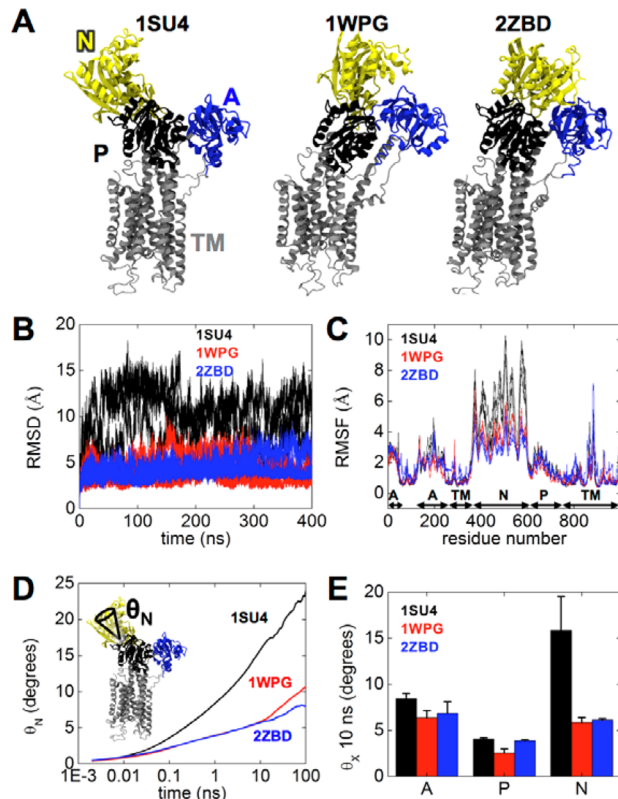


Figure 1. Differential dynamics of SERCA structural substates. (A) Starting structures for AAMD simulations, showing the relative positions of three cytoplasmic domains: actuator (A, blue), nucleotide-binding (N, yellow), phosphorylation (P, black), and the transmembrane domain (TM, gray). (B) Overall C^α RMSD of SERCA. The open conformation (1SU4) showed higher RMSD values and large fluctuations in RMSD. (C) Quantification of RMSF of C^α atoms revealed that the nucleotide-binding (N) domain was the most mobile part of SERCA, with relative structural dynamics $2\text{ZBD} < 1\text{WPG} \ll 1\text{SU4}$. (D) Angular autocorrelation of the N-domain over a range of time scales. The inset represents angular displacement as a wobble cone originating at the hinge of the domain. (E) Summary of SERCA cytoplasmic domain dynamics in the 10 ns time regime. Data are mean \pm SD. Overall, disorder is increased for the open structure (1SU4), especially in the N-domain.

transitions,^{19,20} revealing how mutations may alter transition kinetics. For example, CGMD provided a structural mechanism that explained previous biochemistry experiments²³ in which insertions in the M3 linker decreased the rate of the E1P to E2P transition. This observation could be attributed to accumulation of water around the insertion region, increasing the stability of the E1 state.¹⁹ Together, the results underscore the value of MD simulations for discovering new structures and for investigating the motions of those structures. In many of these studies, attention has justifiably centered on the TM domain where the active sites for ion binding are located. However, TM domain active sites are structurally and functionally coupled to the cytoplasmic domains,^{15,17,24} so there is also great interest in understanding how the A-, N-, and P-domains move and interact during transport.

In the present study, we characterize the dynamics of SERCA in different structural substates using MD simulations starting from X-ray crystal structures determined for SERCA enzymatic substates E1-Ca (1SU4), E2-P (1WPG), and E1P-ADP (2ZBD)^{8,11} (Figure 1A). These structures were chosen to

represent the extremes of the range of SERCA headpiece conformations from open (1SU4) to closed (1WPG, 2ZBD). The goal of these experiments is to test the hypothesis that SERCA conformational fluctuations vary according to the catalytic substates of the pump^{13,25} and identify structural mechanisms for the differential dynamics of enzymatic substates. The results of MD simulations are compared with our previous study in which we used intramolecular FRET between the N- and A-domains as an index of headpiece conformation. Those experiments revealed four discrete structural substates of SERCA expressed in cardiac muscle cells, including several conformations not yet accounted for by published high-resolution structural data. The present MD experiments reveal structural ensembles compatible with those fluorescent measurements and provide insight into the structural details of SERCA domain dynamics. Specifically, we report a structural mechanism that could account for our previous observation that SERCA dynamic disorder decreased with decreasing domain–domain separation distance.

METHODS

Coarse-Grained Simulations of Two-Color SERCA.

Crystal structures of the SERCA were obtained from the RCSB Protein Data Bank²⁶ (PDB entries 1SU4,⁸ 1WPG¹¹ and 2ZBD¹¹) (Figure 1). SERCA structures labeled with fluorescent protein tags were generated using FPMOD²⁷ and were kindly provided by David D. Thomas and Bengt Svensson, University of Minnesota. Molecular dynamics simulations were performed with the GROMACS software package^{28,29} using MARTINI coarse grained force field^{30,31} and domELNEDIN setup,³² which allows cytoplasmic domains move freely. The crystal structures were energy minimized in vacuum to eliminate unfavorable interactions, then two-color SERCA was placed into a palmitoyl-oleoyl-phosphatidyl-choline (POPC) lipid bilayer. Lipids overlapping with the TM-domain of SERCA were removed. Standard cutoff schemes for the MARTINI model were used for the nonbonded interactions. Nonbonded interactions were calculated with a cutoff of 12 Å, on which a shift function was applied, starting at 9 Å for the Lennard-Jones potential and at 0 Å for the electrostatic potential. Charges were screened with a relative dielectric constant $\epsilon_{\text{rel}} = 15$. Simulations were run in the NPT ensemble with pressure 1 bar and temperature 300 K using Berendsen thermostat and barostat.³³ Systems were simulated for 4 μ s using a 20 fs time step.

Atomistic Simulations of SERCA. All-atom MD (AAMD) simulations were carried out using the GROMACS software package^{27,28} with the CHARMM 27 force field^{34–36} and TIP3P water model.³⁷ Energy minimization was performed on the crystal structures using the steepest descent method for 1000 steps, then each model was embedded into a POPC lipid bilayer and solvated in a rectangular water box size with dimensions 130 Å \times 130 Å \times 160 Å. Na⁺ and Cl⁻ ions were added to the solution to neutralize the charge of the system and to produce an ion concentration of 150 mM. The Particle Mesh Ewald method^{38,39} was used to calculate the long-range electrostatic interactions and cutoff of 12 Å was used for the short-range. van der Waals interactions were reduced to zero by switch truncation applied from 8 to 12 Å. Simulations were carried out with an integration time step of 2 fs. To heat the system from 0 K to the target temperature (300 K) and reach the target pressure (1 bar), the Berendsen method was used with relaxation times of 0.1 ps.³³ After 1 ns equilibration, the production run was performed in the NPT ensemble using the

Table 1. Summary of Molecular Dynamics Simulations

method	starting structure	number of trajectories	length of simulation	comments
AAMD	1SU4	4	400 ns	Includes transition trajectory 1SU4*
	1WPG	3	400 ns	
	2ZBD	3	400 ns	
AAMD	WT	6	40 ns	Repeated simulations starting from H-bonded intermediate of transition trajectory 1SU4*
	AAA	6	40 ns	
CGMD	1SU4	1	4 μ s	The distance between the centers of mass of the N and A-domains was harmonically constrained to designated distances between 40 to 30 \AA .
	1WPG	1	4 μ s	
	2ZBD	1	4 μ s	
CGMD	Intermediate structures derived from the open crystal structure 1SU4.	11	1 μ s	

Nose–Hoover thermostat^{40,41} and the Parrinello–Rahman barostat^{42,43} with relaxation times of 1.0 ps. Each independent production run was started with a different set of assigned velocities corresponding to 300 K. The atoms coordinates of the trajectories were saved every 1 ps. The production runs were carried out for 400 ns.

Principal Component Analysis. We used principal component analysis (PCA) to extract the essential motions sampled by the MD trajectory.^{44–46} The set of principal components is the solution to the eigenvalue problem (eq 1), in which the second-moment matrix, \mathbf{A} , contains the mass-weighted internal atomic displacements. The elements of the matrix, A_{ij} , are given by

$$A_{ij} = \sqrt{m_i m_j} \cdot \langle (\vec{r}_i - \bar{r}_i)(\vec{r}_j - \bar{r}_j) \rangle \quad (1)$$

where m_i are the masses. The angular brackets denote time averages. The diagonalization of \mathbf{A} yields the eigenvectors, \mathbf{w}_k , that is, the principal components, and their associated eigenvalues, ξ_k .

Correlation Analysis. To estimate disorder dynamics of SERCA domains we performed correlation analysis of the domain orientation. We quantified the orientation of the vector (where x is N, P, or A), which connects the domain hinge point and middle of the domain. We computed the domain disorder function $\theta_x(t)$ defined as

$$\theta_x(t) = \left\langle \cos^{-1} \left(\frac{\vec{q}_x(0) \cdot \vec{q}_x(t)}{|\vec{q}_x(0)| \cdot |\vec{q}_x(t)|} \right) \right\rangle \quad (2)$$

In fact, $\theta_x(t)$ describes how orientation of domain changed relative to initial one. The angular brackets denote average over time origin. $\theta_x(t)$ can be used to estimate wobble cone of the probe during experiments.

Table 1 provides a summary of the type, duration, and starting conditions for the molecular dynamics simulations.

RESULTS AND DISCUSSION

All-Atom Molecular Dynamics Simulations of SERCA

Motions. To study the differential dynamics of open and closed conformations of the SERCA cytoplasmic headpiece we performed three or four independent 400 ns all-atom molecular dynamics (AAMD) simulations of SERCA for each of three crystal structures, 1SU4, 1WPG, and 2ZBD. Figure 1B shows root-mean square deviations (RMSD) of simulations of open and closed/compact structures of the SERCA as a function of time. Three repeated simulations starting from the open conformation (1SU4, three black traces) showed evidence of

structural disorder compared to three repeated simulations of each of the closed/compact structures (1WPG, red, and 2ZBD, blue). Residue-by-residue analysis of structural fluctuations showed that the difference in dynamics of open and closed conformational substates of SERCA was due primarily to high root-mean-square fluctuations (RMSF) of the 1SU4 N-domain (Figure 1C). For all structures, we observed large RMSF values for the cytoplasmic domains A, N, and P and solvent exposed TM bundle loops compared to TM-domain residues, which is in agreement with previous molecular dynamics simulations studies.^{17,47} Another group's previous studies quantified SERCA domain disorder by measuring the "wobble cone" of a phosphorescent probe. This parameter describes the angles sampled by the probe on a submicrosecond to microsecond time scale, integrating motions that include domain motions and the independent mobility of the phosphorescent probe.⁴⁸ Here, we obtained analogous information for the nanosecond time scale by way of a correlation analysis of the vectors that connect the hinge point of the domains (A-domain, residue 128; N-domain, residue 360; P-domain, residue 328) with the domain center of mass. We quantified the disorder of domains over a range of time scales, calculating a wobble cone angle (θ) from 1 ps to 100 ns. Small values of θ reflect static domains and high values represent mobile (dynamic) domains. The insert in Figure 1D shows a schematic cartoon of the N-domain cone angle. For all domains, the range of angles sampled increases at longer time scales and is presumed to increase further at time scales longer than the 100 ns regime simulated here. Correlation functions for the N-domain for different starting conformations revealed increased dynamic disorder of the open conformation of the pump (1SU4) compared to closed structures (2ZBD, 1WPG) on time scales greater than 0.1 ns (Figure 1D). Figure 1E summarizes the average value of $\theta \pm \text{SD}$ at 10 ns for all three starting conformations average over three independent runs. Consistent with other studies^{17,22} we observed high dynamics for the N-domain, which is significantly more mobile in the open conformation (1SU4) versus closed structures. The P-domain was comparatively static for all structures.

Fundamental Motions of SERCA Cytoplasmic Domains. Principal component analysis (PCA) of AAMD simulations revealed the major modes of such internal dynamics. Overall, the principal components observed here are in agreement with those reported in reference,¹⁷ showing rotational and translational motion of N- and A-domains. Figure 2A shows the three largest-contributing principal components (PCs) for the open and closed conformations of SERCA. Closed conformations (Figure 2A, 1WPG, 2ZBD)

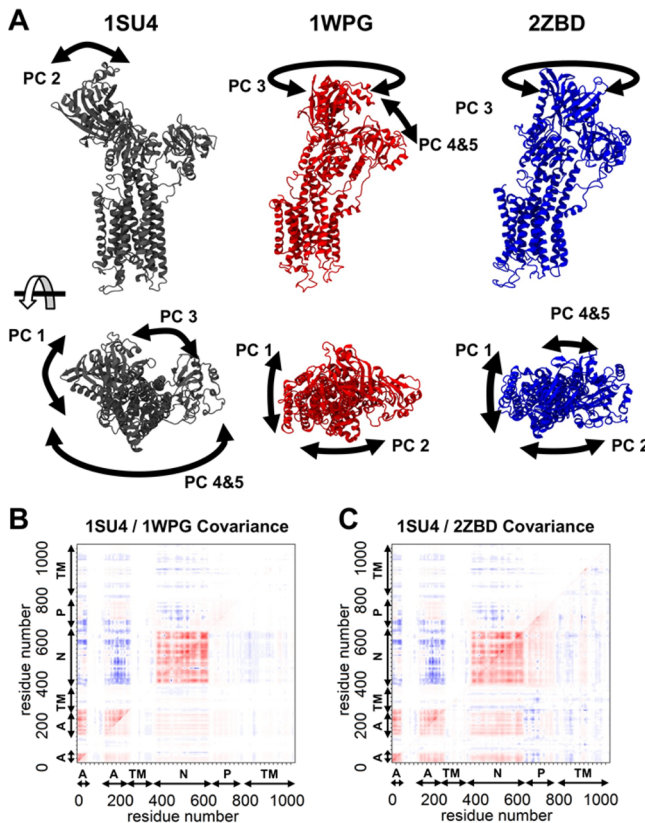


Figure 2. Principal components of SERCA structural dynamics. (A) PCA revealed large relative motions of SERCA cytoplasmic domains for the open structure (1SU4), while close conformations were dominated by concerted motions of the domains as a single unit. (B) Covariance matrices revealed positively correlated (red) and anticorrelated (blue) motions of residues (measured from $C\alpha$) comparing 1SU4 (upper left) with 1WPG (lower right). (C) Covariance analysis, comparing 1SU4 (upper left) and 2ZBD (lower right). Overall, 1SU4 was the most dynamic, showing paradoxical (anticorrelated) motions of the A and N domains.

were characterized by macroscopic motions of the cytoplasmic headpiece as a single unit (PC1, PC2, and PC3) that represented ~65% of internal displacement. These components were present in the open structure (Figure 2A, 1SU4) as well, but they were insignificant compared to large motions of the cytoplasmic domains relative to one another (Figure 2 upper left, 1SU4). For the open structure, PC1 and PC2 were determined to be a motion of the N-domain with respect to the P-domain, opening and closing the nucleotide-binding cleft (67% of internal displacement). PC3 was the relative motion of the N- and A-domains (10%). PC4 and PC5 were minor components, twisting of cytoplasmic headpiece (6%). This analysis suggested that the fluorescent protein fusion positions selected for our previous study of two-color SERCA (N-domain residue #509 and A-domain residue #1)⁴⁹ are ideal sites for quantifying the relative motions of SERCA cytoplasmic domains by FRET. PCA analysis also provided a residue-by-residue correlation of SERCA motions. We compared the covariance matrices of the closed structures with the open state matrix. Figure 2B,C represents large amplitude, positively correlated motion (residues moving in the same direction) in red. Negative correlation (blue) indicates residues moving in opposite directions. As expected, all three structures showed significant positive self-correlation of the N-domain residues

(360–600) due to the large collective motions of these residues. We also observed negative correlation of the N and A domains due to the contrary independent motions of these domains relative to one another. Overall motion is reduced for closed conformations, evident as increased null correlation (white). Notably, the A-N correlation (which was negative for the open conformation) was positive for closed structures, especially 2ZBD, indicating that upon headpiece closure these domains become coupled together and move in unison.

Mechanisms of SERCA Conformational Changes. To investigate how SERCA might undergo a conformational change from open structures (such as 1SU4) to compact conformations, we investigated AAMD simulation results in greater detail. Figure 3A shows the time dependent changes in

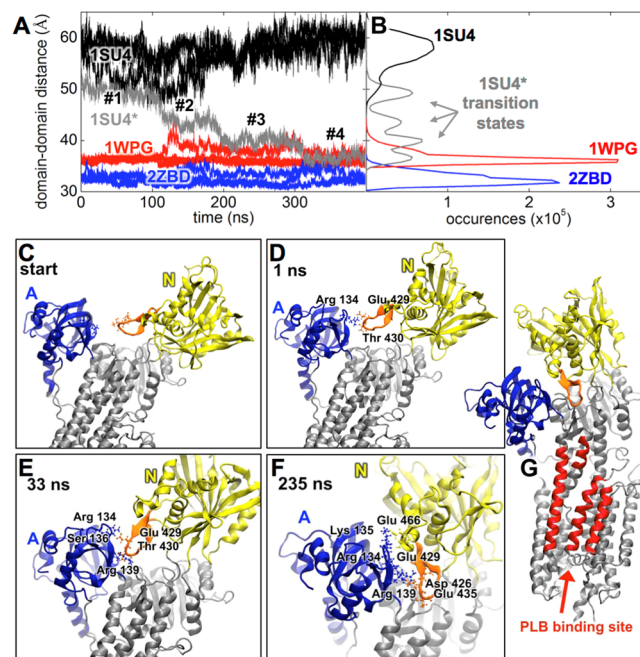


Figure 3. AAMD simulations revealed details of SERCA structural dynamics. (A) Fluctuations in the distance between N and A domains revealed the differences in the dynamics of open and closed conformations. One 1SU4 trajectory (1SU4*, gray) exhibited an open-to-close conformational transition. (B) Histograms of N and A domains separation distances show resolved peaks consistent with discrete structures and intermediate transition states. (C) The starting structure (1SU4) with a widely open cytoplasmic headpiece. (D) At 1 ns, H-bonding stabilized a bridge between the N-domain loop and the A-domain. (E) Rotation of the N-domain and partial closure of the N-A gap. (F) Engagement of additional surfaces on the A- and N-domains stabilized a closed conformation. (G) After headpiece closure the N β 5- β 6 loop pointed toward the inhibitory binding cleft (red), where it could interact with PLB.

domain–domain separation distance, measured from the centers of mass of the A- and N-domains. The data comprise a total of 10 trajectories: 4 replicates starting with 1SU4 (Figure 3A, 3 black and 1 gray), and 3 replicates each for 1WPG (Figure 3A, red) and 2ZBD (Figure 3A, blue). We observed larger, more variable domain separation distances for 1SU4 compared to 1WPG and 2ZBD. The latter two exhibited stable, ordered structures, as shown by flat trajectories with little fluctuation in the domain separation distance. Thus, the simulations recapitulated previous FRET measurements that suggested decreasing disorder as the cytoplasmic headpiece

closes. Interestingly, one of the 1SU4 trajectories showed a progressive closure of the cytoplasmic headpiece over the 400 ns simulation (Figure 3A, gray). This trajectory was characterized by a series of plateaus (Figure 3A, #1–4), suggesting intermediate transition states. Figure 3B shows a histogram of measured domain–domain separation values, revealing the expected narrow distribution of short distances for the closed structures (Figure 3B, blue, red), and longer, more variable distances for the open conformation, as shown by a wide histogram (Figure 3B, black). The histogram of the transition trajectory showed several apparent intermediate conformations visible as multiple discrete peaks (Figure 3B, transition states). A detailed analysis of this trajectory revealed that the cytoplasmic headpiece underwent a progressive stepwise transition to a structure that was as tightly closed as the compact structure of 1WPG. The staircase profile of the trajectory is annotated in Figure 3A to highlight the plateau phases (#1–4). Transitions between these apparent intermediate subconformations were rapid. Early in the transition trajectory we noted an N-domain loop ($N\beta 5-\beta 6$) consisting of residues 426 to 436 that sampled the space between the N- and A-domains (Figure 3C). This loop is near other N-domain residues that are important for interacting with Mg-ATP, such as Glu439.¹² Figure 3C shows that at the beginning of the simulation the headpiece was in the open 1SU4 configuration, but within 1 ns, loop residues Glu 429 and Thr 430 (N-domain) stretched across the gap to form dynamic H-bonds with the A-domain Arg 134 (Figure 3D). In addition, Glu 429 repeatedly formed H-bonds with Lys 135 and Ser 136 in the A domain; the N-domain $N\beta 5-\beta 6$ loop formed a bridge between the domains (Figure 3E). H-bond interactions began to occur in more proximal regions of the loop after 100 ns, contributing to the transition to plateau #2. The domain–domain contact shifted along the surface of the A-domain, drawing the two domains together and rotating the N-domain about the membrane normal axis. The structure sampled during plateau #2 was stabilized by interactions between Arg 139 and Thr 430. The conformation of plateau #3 is shown at 235 ns (Figure 3F). This structure had broadly distributed points of domain–domain interaction, such as Ser 134, Ser 136, and Arg 139 (A-domain) with Glu 466, Ser 463, and Glu 429 (N-domain). By this time, the bridge loop had rotated significantly away from the cleft and was no longer the only point of interaction between the two domains. In particular, Figure 3F shows that Thr 430 points away from the domain–domain interface. This is the most distal residue at the apex of the $N\beta 5-\beta 6$ loop and was one of the first residues to initiate domain–domain H-bonding. In the most compact conformation, corresponding to the fourth plateau, the N-domain/A-domain interface was comparatively stable, and Glu 435 of the N-domain bridge loop interacted with other N-domain residues Asn 428 and Lys 431. The intradomain H-bonding contributed to the prevailing structure of the $N\beta 5-\beta 6$ loop. At the end of the 400 ns simulation, the N-domain A-domain interface was still partly open, and the $N\beta 5-\beta 6$ loop pointed away from the N–A interface. Interestingly, this final orientation could put the loop in a position to interact with phospholamban bound to the SERCA regulatory binding site (Figure 3G, red). Specifically, the acidic residues (which were the first to interact with the A domain) were in a good position to interact with basic residues on the cytoplasmic domain of PLB. This hypothetical interaction could help complete the rotation of the N-domain and the closure of the A–N cleft. The PLB-SERCA regulatory

complex was recently determined,⁵⁰ but structural dynamics prevented the cytoplasmic domain of PLB from being resolved. Thus, it is unknown how PLB (especially phosphorylated PLB) can induce SERCA to assume the highly compact SERCA structure that was observed by single molecule FRET (State IV). In live cells, this unique SERCA structure was only observed in the presence of Ca^{2+} and phosphorylated PLB, suggesting that it represents a disinhibited regulatory complex. It remains to be determined how stabilizing this putative compact intermediate could contribute to improved catalytic efficiency of Ca^{2+} transport.^{51–54} Supporting Information Supplemental Movie 1 shows the structure fluctuations of the 1SU4* trajectory that underwent an open-to-closed transition. The trajectory contrasted with the other 1SU4 simulations in which the headpiece fluctuated about a broad distribution of structures without departing from the overall open configuration (Figure 3A, black traces). Overall, saltatory closure of the headpiece was suggestive of discrete conformational substates, some of which were long-lived with >50 ns dwell times (Figure 3A, gray). To more clearly show the transitions between each plateau, we performed a morph between representative structures (Supporting Information Supplemental Movie 2), however we emphasize that SERCA did not follow a prescribed, orderly path from one static state to the next. Rather, the structural transitions are highly stochastic, and the enzymatic substates are characterized by considerable structural disorder and degeneracy.

The Structural Role of $N\beta 5-\beta 6$ Loop Charged Residues. The open-to-closed transition trajectory was intriguing and suggestive of a structural mechanism by which headpiece closure could be initiated. We tested the reproducibility of this apparently spontaneous conformational transition by performing repeated simulations beginning just after formation of the first H-bonds between the N- and A-domains (Figure 3D). Of six repeated simulations with randomized velocities, four maintained the initial H-bonds that stabilized the relative position of the two domains and two spontaneously progressed toward headpiece closure within 40 ns. The results indicate that the structural transition we observed in trajectory 1SU4* is representative and reproducible. The simulations also suggest that the disorder-to-order transition is a key step for initiation of the open-to-closed conformational change. We hypothesized that key loop residues involved in initial H-bonding were important for stabilizing the relative positions of the domains and initiating headpiece closure. To test this, we mutated residues 426, 429, and 435 to Ala to abolish H-bond interactions. This resulted in destabilization of the headpiece architecture with six simulations of mutated (“AAA”) SERCA showing high variability and disorder compared to WT (Figure 4A). Without the loop residues to initiate contact, the A and N domains were separated by a water cushion (Figure 4B) that was poorly diffusible. For the water model employed here⁵⁵ the diffusion coefficient was $3.2 \pm 0.5 \cdot 10^{-5}$ in the cleft vs $4.6 \pm 0.2 \cdot 10^{-5}$ cm^2/s in bulk solution. Figure 4C shows how the loop residues pierced this cushion to create a hole in the water layer through which domain–domain contact was initiated and expanded (Figure 4D). Mutation of the loop residues to Ala resulted in a rapid loss of domain–domain contacts (Figure 4D).

The Role of the $N\beta 5-\beta 6$ Loop in Ca Transporter Structural Dynamics and Function. The *in vivo* significance of the proposed structural mechanism is suggested by a high degree of $N\beta 5-\beta 6$ loop homology among Ca^{2+} transporters

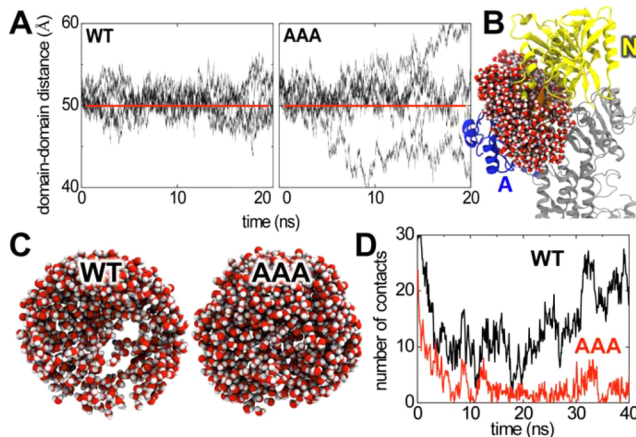


Figure 4. The effect of mutation of loop residues on the SERCA headpiece disorder-to-order transition. (A) WT SERCA H-bonds stabilize the Plateau #1 structure compared to the AAA mutant. (B) A water cushion (spheres) prevents A–N contacts. (C) WT loop residues pierce a hole in the water layer. (D) AAA mutation prevents normal domain interactions (data are mean of six replicates).

Table 2. Conservation of Negatively Charged Loop N β 5- β 6 Residues Across Diverse Taxa

Asp426 Glu429 Glu435	SERCA1a	rabbit
DFNETKGVYEVKVG	SERCA1a	dog
DFNETKGVYEVKVG	SERCA1a	human
DFNEAKGVYEVKVG	SERCA2	frog
DFNEAKGVYEVKVG	SERCA2a	rabbit
DYNEAKGVYEVKVG	SERCA2b	human
DYNEAKGIYEVKVG	SERCA1	chicken
DYNEAKGVYEVKVG	SERCA2	chicken
DYNESKGVYEVKVG	SERCA2	fish
DFNEYKQCFEKVG	SERCA	spider
DFNEVKVFKEKVG	SERCA	mosquito
DYNESKGGLFEKVG	Ca-ATPase	tapeworm
DYNEAKDIYEVKVG	SERCA	oyster
---ETKEIYEKI-	bact cobalt transp.	

from a range of species, including mammals, amphibians, reptiles, birds, fish, and invertebrates (Table 2). The negatively charged loop residues that interacted with positive A-domain residues in our simulations are particularly well-conserved. Some loop residues have already been reported in the literature to be functionally important. For example, N-domain Asp426 and A-domain Arg134 were previously implicated as being interacting residues from crystallography studies,⁵⁶ and we confirmed that these residues interact at latter stages (plateau #3) of the closure transition (Figure 3A). Interestingly, mutation of 426 and 134 to Ala has been shown to decrease ATPase activity by 60 and 35%, respectively,⁵⁶ underscoring the functional importance of interactions between the N β 5- β 6 loop and the A-domain. The present data suggest a key structural role for other loop residues, particularly those involved in stabilizing plateau #1 structure (Figure 3A) during the initiation of domain contact. One interesting residue is Thr430, an important source of early H-bond interactions with Arg134 during the disorder-to-order transition of plateau #1 for the rabbit SERCA1a simulated here. This polar residue is more commonly an Ala in most species and isoforms (Table 2), but

we speculate that Thr may confer a gain of function in the rabbit and dog SERCA1a isoforms. Consistent with this, Inesi and colleagues have shown that the rabbit SERCA1a cycles with ~20% faster kinetics compared to the chicken,⁵⁷ which lacks Thr430. We did not observe similarities between the SERCA N β 5- β 6 loop and other P-type pumps such as PMCA, NKA, copper transporter, or H⁺/K⁺-ATPases. Thus, the putative transition mechanism may be unique to Ca²⁺ transporters.

Comparison of MD Results with Previous Structural Studies.

Some of the simulated conformations approximated existing SERCA crystal structures, as quantified by alignment of the cytoplasmic domains of these structures to conformations sampled during the simulation. While the structures of plateau #1 still mostly closely resembled the starting structure (1SU4), after the transition to plateau #2 the conformation became more similar to E1-Mg (3WSB)⁵⁸ with a difference of ~5 Å RMSD. For comparison, the RMSD of the trajectory versus E2 states (e.g., 1WPG, 1IWO)^{9,11} was ~15 Å. The similarity of the simulated structures to 3WSB was maintained at 5 Å through plateau #3. The structures of plateau #4 were halfway between 3WSB and E1-ATP structures (e.g., 1TST, 1VFP, 2ZBD).^{11,59} None of the X-ray crystal structures have captured the dynamic hydrogen bonding of the N β 5- β 6 loop to the A-domain that was observed in the early stages of the AAMD simulation (Figure 4D,E). The range of structures sampled during AAMD simulations is represented in (Figure 5). The decrease in disorder with cytoplasmic headpiece closure was evident from a comparison of these structure families. There was tighter backbone superimposition as SERCA progresses from open (left) to closed (right) conformations. 1SU4 showed the greatest diversity of structures (Figure 5A), consistent with increased disorder for this open conformation. A family of structures representing the transitional substate of plateau #2 (Figure 3A) is shown in Figure 5B, and represents a partially closed conformation that is intermediate between open 1SU4 (Figure 3A) and closed 1WPG (Figure 3C). This putative transition state (Figure 3B, gray) showed a level of disorder that was intermediate between the open (1SU4, black) and closed (1WPG, red) conformations. The tightly closed conformation of 2ZBD (Figure 5D) yielded an orderly array of similar compact structures. This high degree of structural order may make these conformations easier to crystallize, and most X-ray structures have a compact cytoplasmic headpiece. Only one has been solved for the open conformation¹¹ and intermediate structures (Figure 5B) have not been observed yet.

The present observations may also be compared to our previous intramolecular FRET measurements.¹³ One caveat for such an analysis is that the two techniques explore time regimes differing by 2–3 orders of magnitude. However, some substates were stable for the entire 400 ns simulation (Figure 3A) and might still be represented on the μ s-ms time scale of the fluorescence measurements.¹³ To determine how GFP-tagRFP FRET distances would be changed by structural dynamics that alter N-A distance, we performed CGMD simulations of two-color SERCA (Figure 5E). CGMD experiments recapitulated observations from AAMD and FRET experiments, showing increased dynamics of open structures compared to compact conformations. In addition, we analyzed the distances between centers of mass of GFP and the N-domain, tagRFP and the A-domain, the A- and N-domains, and between the fluorescent probes tagRFP and GFP (FRET distance). For all starting crystal structures (1SU4, 1WPG, and 2ZBD), the distance between the fluorescent protein and the domain to which it was

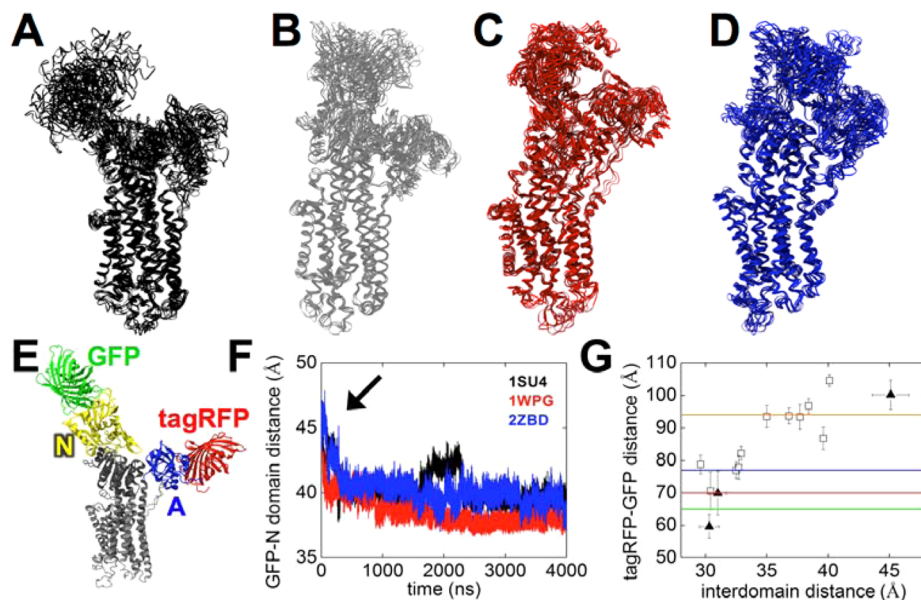


Figure 5. Comparison of MD simulation results with previous structural studies. (A) A representative sample of structures assumed for the open conformation (1SU4), excluding the transition trajectory. (B) Structures sampled during plateau #2 of the transition trajectory. (C) Structures sampled by 1WPG. (D) Structures sampled by 2ZBD. (E) “Two-color SERCA”, a construct that reports SERCA structural dynamics with FRET changes. (F) CGMD revealed that the distance between the N-domain and GFP decreased early in the simulation (at arrow), consistent with docking of the fluorescent protein to the domain to which it was attached. (G) There was a positive correlation between the separation of fluorescent proteins and the distance between domains. Filled triangles represent CGMD simulations started from crystal structures and open squares show results from harmonically constrained simulations. Horizontal lines represent discrete conformational substates previously detected as resolved populations in a FRET efficiency histogram.

attached decreased rapidly (Figure 5F, at arrow) as the fluorescent protein settled onto and stably interacted with the surface of the target domain. The final GFP-tagRFP separation and interdomain distances depended on the starting conformation of the SERCA pump. A comparison of stabilized structures revealed a positive relationship between fluorescent protein separation and domain–domain distance (Figure 5G). Because unconstrained CGMD simulations did not fully sample the entire range of possible distances, we used the open structure (1SU4) as a starting point and generated 11 new intermediate structures. These intermediate conformations were harmonically restrained to represent domain separation distances from 30 to 40 Å (in 1 Å increments). CGMD simulations of these new starting structures populated the gap between open and closed SERCA structures in the plot of fluorescent protein separation vs domain separation (Figure 5G, open squares). Overall, we conclude that the fluorescent protein tags are closely associated with the target domains and FRET is a good index of the overall headpiece conformation. The previously observed FRET substates are represented in Figure 5G as horizontal lines (I orange, 94 Å; II blue, 77 Å; III red, 70 Å; IV green, 65 Å).¹³ The relationship of Figure 5G is useful as a guide for comparison of the present simulations with previous FRET experiments. For example, we regard domain separation distances of the structures sampled by 1SU4 as comparable to FRET State I.¹³ Specifically, the 1SU4 AAMD simulation (Figure 3A, black) yielded domain–domain distances of 35–60 Å, which corresponds to fluorescent protein separation distances greater than 90 Å according to the relationship in Figure 5G. This prediction is compatible with the broad FRET distribution and low FRET efficiency observed for State I.¹³ The fluorescent protein separation distance of that state was too long to measure with the Cer-YFP

FRET pair but changing to the GFP-tagRFP pair yielded a State I distribution center value of 5% FRET. This corresponds to a probe separation distance of 94 Å for State I,¹³ which compares favorably with the AAMD prediction of distances greater than 90 Å for the open 1SU4 structure. The decreased domain–domain separation of 33 Å observed for 2ZBD (Figure 3A) would be expected to yield fluorescent protein separations of ~75 Å according to the relationship in Figure 5G. This is in the range of distances calculated for FRET States II and III, which were 78 and 69 Å for the Cer-YFP pair and 77 and 70 Å for the GFP-tagRFP pair.¹³ Very compact structures corresponding to State IV were not observed. Figure 5G indicates fluorescent protein separation distances of 62–65 Å¹³ should arise from domain separation distances of less than 30 Å, which were not detected in AAMD experiments (Figure 3A). This is not unexpected, as this very high FRET compact state is only observed when SERCA is bound to phosphorylated PLB, and PLB was not present in the simulations.

Summary. Overall, the simulations complement the FRET measurements and support hypotheses generated from those previous experiments. Specifically, the simulations confirmed that SERCA structural disorder decreases as the headpiece closes, as shown by analysis of structure fluctuations (Figure 1), domain separation distance (Figure 3A,B), principal component analysis (Figure 2), and correlation analysis of domain angular disorder (Figure 1D). We attribute this disorder-to-order transition to interactions between acidic residues of the N-domain N β 5– β 6 loop and basic residues on the A-domain (Figure 3). Mutation of several key residues (Asp426, Glu429, and Glu435) to Ala prevented these interactions, destabilizing the relative positions of the N- and A-domains. The simulations suggest that these H-bonds are formed early in the open-to-closed transition and help overcome the energy barrier of a

poorly diffusible cushion of water to facilitate the closure of the cytoplasmic headpiece during the Ca^{2+} transport cycle. The high degree of conservations of residues implicated in SERCA headpiece closure suggests that this putative mechanism may be a general feature of the transport cycle for a wide range of Ca^{2+} transporters.

■ ASSOCIATED CONTENT

Supporting Information

Supporting Movie 1: An MD simulation reveals SERCA conformational fluctuations and an open-to-closed transition. Supporting Movie 2: A morph movie revealing the transitions between conformational substates during the closure of the SERCA cytoplasmic headpiece. This material is available free of charge via the Internet at <http://pubs.acs.org>.

■ AUTHOR INFORMATION

Corresponding Author

*E-mail: srobia@luc.edu. Phone: (708) 216-2522.

Notes

The authors declare no competing financial interest.

■ ACKNOWLEDGMENTS

The authors thank David D. Thomas, Bengt Svensson, L. Michel Espinoza-Fonseca, Avisek Das, J. Michael Autry and Peter M. Kekenes-Huskey for stimulating discussions. Also we would like to thank David D. Thomas and Bengt Svensson for providing two-color SERCA starting structures. We thank Shadman Jubaer for technical assistance. This work used the Extreme Science and Engineering Discovery Environment (XSEDE), which is supported by National Science Foundation Grant OCI-1053575. This research was supported by National Institute of Health Grant HL106189 and by equipment and facilities provided by National Institute of Health grant "Loyola Research Computing Core" 1G20RR030939.

■ REFERENCES

- (1) MacLennan, D. H.; Rice, W. J.; Green, N. M. The Mechanism of Ca^{2+} Transport by Sarco(Endo)Plasmic Reticulum Ca^{2+} -ATPases. *J. Biol. Chem.* **1997**, *272*, 28815–28818.
- (2) Biehl, R.; Hoffmann, B.; Monkenbusch, M.; Falus, P.; Preost, S.; Merkel, R.; Richter, D. Direct Observation of Correlated Interdomain Motion in Alcohol Dehydrogenase. *Phys. Rev. Lett.* **2008**, *101*, 138102.
- (3) Henzler-Wildman, K. A.; Thai, V.; Lei, M.; Ott, M.; Wolf-Watz, M.; Fenn, T.; Pozharski, E.; Wilson, M. A.; Petsko, G. A.; Karplus, M.; Hubner, C. G.; Kern, D. Intrinsic Motions Along an Enzymatic Reaction Trajectory. *Nature* **2007**, *450*, 838–844.
- (4) Bu, Z. M.; Biehl, R.; Monkenbusch, M.; Richter, D.; Callaway, D. J. E. Coupled Protein Domain Motion in Taq Polymerase Revealed by Neutron Spin-Echo Spectroscopy. *Proc. Natl. Acad. Sci. U.S.A.* **2005**, *102*, 17646–17651.
- (5) Gerstein, M.; Lesk, A. M.; Chothia, C. Structural Mechanisms for Domain Movements in Proteins. *Biochemistry* **1994**, *33*, 6739–6749.
- (6) Case, D. A. Normal-Mode Analysis of Protein Dynamics. *Curr. Opin. Struct. Biol.* **1994**, *4*, 285–290.
- (7) Bennett, W. S., Jr.; Steitz, T. A. Glucose-Induced Conformational Change in Yeast Hexokinase. *Proc. Natl. Acad. Sci. U.S.A.* **1978**, *75*, 4848–4852.
- (8) Toyoshima, C.; Nakasako, M.; Nomura, H.; Ogawa, H. Crystal Structure of the Calcium Pump of Sarcoplasmic Reticulum at 2.6 Ångstrom Resolution. *Nature* **2000**, *405*, 647–655.
- (9) Toyoshima, C.; Nomura, H. Structural Changes in the Calcium Pump Accompanying the Dissociation of Calcium. *Nature* **2002**, *418*, 605–611.
- (10) Olesen, C.; Picard, M.; Winther, A. M. L.; Gyurp, C.; Morth, J. P.; Osvig, C.; Møller, J. V.; Nissen, P. The Structural Basis of Calcium Transport by the Calcium Pump. *Nature* **2007**, *450*, 1036–U1035.
- (11) Toyoshima, C.; Nomura, H.; Tsuda, T. Luminal Gating Mechanism Revealed in Calcium Pump Crystal Structures with Phosphate Analogue. *Nature* **2004**, *432*, 361–368.
- (12) Jensen, A. M. L.; Sorensen, T. L. M.; Olesen, C.; Møller, J. V.; Nissen, P. Modulatory and Catalytic Modes of ATP Binding by the Calcium Pump. *EMBO J.* **2006**, *25*, 2305–2314.
- (13) Pallikkuth, S.; Blackwell, Daniel J.; Hu, Z.; Hou, Z.; Zieman, Dane T.; Svensson, B.; Thomas, David D.; Robia, Seth L. Phosphorylated Phospholamban Stabilizes a Compact Conformation Of the Cardiac Calcium-ATPase. *Biophys. J.* **2013**, *105*, 1812–1821.
- (14) Sugita, Y.; Ikeguchi, M.; Toyoshima, C. Relationship between Ca^{2+} -Affinity and Shielding of Bulk Water in the Ca^{2+} -Pump from Molecular Dynamics Simulations. *Proc. Natl. Acad. Sci. U.S.A.* **2010**, *107*, 21465–21469.
- (15) Espinoza-Fonseca, L. M.; Thomas, D. D. Atomic-Level Characterization of the Activation Mechanism of SERCA by Calcium. *PLoS One* **2011**, *6*, e26936.
- (16) Musgaard, M.; Thogersen, L.; Schiott, B. Protonation States of Important Acidic Residues in the Central Ca^{2+} Ion Binding Sites of the Ca^{2+} -ATPase: A Molecular Modeling Study. *Biochemistry* **2011**, *50*, 11109–11120.
- (17) Kekenes-Huskey, P. M.; Metzger, V. T.; Grant, B. J.; McCammon, J. A. Calcium Binding and Allosteric Signaling Mechanisms for the Sarcoplasmic Reticulum Ca^{2+} ATPase. *Protein Sci.* **2012**, *21*, 1429–1443.
- (18) Musgaard, M.; Thogersen, L.; Schiott, B.; Tajkhorshid, E. Tracing Cytoplasmic Ca^{2+} Ion and Water Access Points in the Ca^{2+} -Atpase. *Biophys. J.* **2012**, *102*, 268–277.
- (19) Nagarajan, A.; Andersen, J. P.; Woolf, T. B. Coarse-Grained Simulations of Transitions in the E2-to-E1 Conformations for Ca ATPase (SERCA) Show Entropy-Enthalpy Compensation. *J. Mol. Biol.* **2012**, *422*, 575–593.
- (20) Nagarajan, A.; Andersen, J. P.; Woolf, T. B. The Role of Domain: Domain Interactions Versus Domain: Water Interactions in the Coarse-Grained Simulations of the E1p to E2p Transitions in Ca-Atpase (SERCA). *Proteins: Struct. Funct. Bioinform.* **2012**, *80*, 1929–1947.
- (21) Espinoza-Fonseca, L. M.; Autry, J. M.; Thomas, D. D. Microsecond Molecular Dynamics Simulations of Mg^{2+} - and K^{+} -Bound E1 Intermediate States of the Calcium Pump. *PLoS One* **2014**, *9*, e95979.
- (22) Das, A.; Gur, M.; Cheng, M. H.; Jo, S.; Bahar, I.; Roux, B. Exploring the Conformational Transitions of Biomolecular Systems Using a Simple Two-State Anisotropic Network Model. *PLoS Comp. Biol.* **2014**, *10*, e1003521.
- (23) Holdensen, A. N.; Andersen, J. P. The Length of the a-M3 Linker Is a Crucial Determinant of the Rate of the Ca^{2+} Transport Cycle of Sarcoplasmic Reticulum Ca^{2+} -Atpase. *J. Biol. Chem.* **2009**, *284*, 12258–12265.
- (24) Møller, J. V.; Olesen, C.; Winther, A. M. L.; Nissen, P. The Sarcoplasmic Ca^{2+} -Atpase: Designof a Perfect Chemi-Osmotic Pump. *Q. Rev. Biophys.* **2010**, *43*, 501–566.
- (25) Inesi, G.; Lewis, D.; Toyoshima, C.; Hirata, A.; de Meis, L. Conformational Fluctuations of the Ca^{2+} -Atpase in the Native Membrane Environment - Effects of Ph, Temperature, Catalytic Substrates, and Thapsigargin. *J. Biol. Chem.* **2008**, *283*, 1189–1196.
- (26) Bernstein, F. C.; Koetzle, T. F.; Williams, G. J.; Meyer, E. F., Jr.; Brice, M. D.; Rodgers, J. R.; Kennard, O.; Shimomouchi, T.; Tasumi, M. The Protein Data Bank: A Computer-Based Archival File for Macromolecular Structures. *J. Mol. Biol.* **1977**, *112*, 535–542.
- (27) Pham, E.; Chiang, J.; Li, I.; Shum, W.; Truong, K. A Computational Tool for Designing Fret Protein Biosensors by Rigid-Body Sampling of Their Conformational Space. *Structure* **2007**, *15*, 515–523.

- (28) Hess, B.; Kutzner, C.; van der Spoel, D.; Lindahl, E. Gromacs 4: Algorithms for Highly Efficient, Load-Balanced, and Scalable Molecular Simulation. *J. Chem. Theory Comput.* **2008**, *4*, 435–447.
- (29) Pronk, S.; Pall, S.; Schulz, R.; Larsson, P.; Bjelkmar, P.; Apostolov, R.; Shirts, M. R.; Smith, J. C.; Kasson, P. M.; van der Spoel, D.; Hess, B.; Lindahl, E. Gromacs 4.5: A High-Throughput and Highly Parallel Open Source Molecular Simulation Toolkit. *Bioinformatics* **2013**, *29*, 845–854.
- (30) Monticelli, L.; Kandasamy, S. K.; Periole, X.; Larson, R. G.; Tielemans, D. P.; Marrink, S. J. The Martini Coarse-Grained Force Field: Extension to Proteins. *J. Chem. Theory Comput.* **2008**, *4*, 819–834.
- (31) de Jong, D. H.; Singh, G.; Bennett, W. F. D.; Arnarez, C.; Wassenaar, T. A.; Schafer, L. V.; Periole, X.; Tielemans, D. P.; Marrink, S. J. Improved Parameters for the Martini Coarse-Grained Protein Force Field. *J. Chem. Theory Comput.* **2013**, *9*, 687–697.
- (32) Siuda, I.; Thøgersen, L. Conformational Flexibility of the Leucine Binding Protein Examined by Protein Domain Coarse-Grained Molecular Dynamics. *J. Mol. Model.* **2013**, *19*, 4931–4945.
- (33) Berendsen, H. J. C.; Postma, J. P. M.; Gunsteren, W. F. v.; DiNola, A.; Haak, J. R. Molecular Dynamics with Coupling to an External Bath. *J. Chem. Phys.* **1984**, *81*, 3684–3690.
- (34) MacKerell, A. D.; Feig, M.; Brooks, C. L. Extending the Treatment of Backbone Energetics in Protein Force Fields: Limitations of Gas-Phase Quantum Mechanics in Reproducing Protein Conformational Distributions in Molecular Dynamics Simulations. *J. Comput. Chem.* **2004**, *25*, 1400–1415.
- (35) MacKerell, A. D.; Feig, M.; Brooks, C. L. Improved Treatment of the Protein Backbone in Empirical Force Fields. *J. Am. Chem. Soc.* **2004**, *126*, 698–699.
- (36) Foloppe, N.; MacKerell, A. D. All-Atom Empirical Force Field for Nucleic Acids: I. Parameter Optimization Based on Small Molecule and Condensed Phase Macromolecular Target Data. *J. Comput. Chem.* **2000**, *21*, 86–104.
- (37) Jorgensen, W. L.; Chandrasekhar, J.; Madura, J. D.; Impey, R. W.; Klein, M. L. Comparison of Simple Potential Functions for Simulating Liquid Water. *J. Chem. Phys.* **1983**, *79*, 926–935.
- (38) Darden, T.; York, D.; Pedersen, L. Particle Mesh Ewald - an N.Log(N) Method for Ewald Sums in Large Systems. *J. Chem. Phys.* **1993**, *98*, 10089–10092.
- (39) Essmann, U.; Perera, L.; Berkowitz, M. L.; Darden, T.; Lee, H.; Pedersen, L. G. A Smooth Particle Mesh Ewald Method. *J. Chem. Phys.* **1995**, *103*, 8577–8593.
- (40) Hoover, W. G. Canonical Dynamics - Equilibrium Phase-Space Distributions. *Phys. Rev. A: At. Mol. Opt. Phys.* **1985**, *31*, 1695–1697.
- (41) Nose, S. A Molecular-Dynamics Method for Simulations in the Canonical Ensemble. *Mol. Phys.* **1984**, *52*, 255–268.
- (42) Nose, S.; Klein, M. L. Constant Pressure Molecular-Dynamics for Molecular-Systems. *Mol. Phys.* **1983**, *50*, 1055–1076.
- (43) Parrinello, M.; Rahman, A. Polymorphic Transitions in Single-Crystals - a New Molecular-Dynamics Method. *J. Appl. Phys.* **1981**, *52*, 7182–7190.
- (44) Tournier, A. L.; Smith, J. C. Principal Components of the Protein Dynamical Transition. *Phys. Rev. Lett.* **2003**, *91*, 208106.
- (45) Kitao, A.; Hayward, S.; Go, N. Energy Landscape of a Native Protein: Jumping-among-Minima Model. *Proteins: Struct., Funct., Genet.* **1998**, *33*, 496–517.
- (46) Karplus, M.; Kushick, J. N. Method for Estimating the Configurational Entropy of Macromolecules. *Macromolecules* **1981**, *14*, 325–332.
- (47) Costa, V.; Carloni, P. Calcium, Binding to the Transmembrane Domain of the Sarcoplasmic Reticulum Ca^{2+} -ATPase: Insights from Molecular Modeling. *Proteins: Struct., Funct., Genet.* **2003**, *50*, 104–113.
- (48) Mueller, B.; Zhao, M.; Negashov, I. V.; Bennett, R.; Thomas, D. D. SERCA Structural Dynamics Induced by ATP and Calcium. *Biochemistry* **2004**, *43*, 12846–12854.
- (49) Hou, Z. J.; Hu, Z. H.; Blackwell, D. J.; Miller, T. D.; Thomas, D. D.; Robia, S. L. 2-Color Calcium Pump Reveals Closure of the Cytoplasmic Headpiece with Calcium Binding. *PLoS One* **2012**, *7*, e40369.
- (50) Akin, B. L.; Hurley, T. D.; Chen, Z.; Jones, L. R. The Structural Basis for Phospholamban Inhibition of the Calcium Pump in Sarcoplasmic Reticulum. *J. Biol. Chem.* **2013**, *288*, 30181–30191.
- (51) Mahaney, J. E.; Albers, R. W.; Waggoner, J. R.; Kutchai, H. C.; Froehlich, J. P. Intermolecular Conformational Coupling and Free Energy Exchange Enhance the Catalytic Efficiency of Cardiac Muscle SERCA2a Following the Relief of Phospholamban Inhibition. *Biochemistry* **2005**, *44*, 7713–7724.
- (52) Frank, K.; Tilgmann, C.; Shannon, T. R.; Bers, D. M.; Kranias, E. G. Regulatory Role of Phospholamban in the Efficiency of Cardiac Sarcoplasmic Reticulum Ca^{2+} Transport. *Biochemistry* **2000**, *39*, 14176–14182.
- (53) Shannon, T. R.; Chu, G. X.; Kranias, E. G.; Bers, D. M. Phospholamban Decreases the Energetic Efficiency of the Sarcoplasmic Reticulum Ca Pump. *J. Biol. Chem.* **2001**, *276*, 7195–7201.
- (54) Antipenko, A. Y.; Spielman, A. I.; Sassaroli, M.; Kirchberger, M. A. Comparison of the Kinetic Effects of Phospholamban Phosphorylation and Anti-Phospholamban Monoclonal Antibody on the Calcium Pump in Purified Cardiac Sarcoplasmic Reticulum Membranes. *Biochemistry* **1997**, *36*, 12903–12910.
- (55) Mahoney, M. W.; Jorgensen, W. L. Diffusion Constant of the TipSp Model of Liquid Water. *J. Chem. Phys.* **2001**, *114*, 363–366.
- (56) Ma, H.; Lewis, D.; Xu, C.; Inesi, G.; Toyoshima, C. Functional and Structural Roles of Critical Amino Acids within the “N”, “P”, and “A” Domains of the Ca^{2+} ATPase (SERCA) Headpiece. *Biochemistry* **2005**, *44*, 8090–8100.
- (57) Sumbilla, C.; Cavagna, M.; Zhong, L. L.; Ma, H. L.; Lewis, D.; Farrance, I.; Inesi, G. Comparison of SERCA1 and SERCA2a Expressed in Cos-1 Cells and Cardiac Myocytes. *American Journal of Physiology-Heart and Circulatory Physiology* **1999**, *277*, H2381–H2391.
- (58) Toyoshima, C.; Iwasawa, S.; Ogawa, H.; Hirata, A.; Tsueda, J.; Inesi, G. Crystal Structures of the Calcium Pump and Sarcolipin in the Mg^{2+} -Bound E1 State. *Nature* **2013**, *495*, 260–264.
- (59) Sorensen, T. L. M.; Møller, J. V.; Nissen, P. Phosphoryl Transfer and Calcium Ion Occlusion in the Calcium Pump. *Science* **2004**, *304*, 1672–1675.